Geophysical Research Letters

Supporting Information for

Large modeling uncertainty in projecting decadal surface ozone changes over city clusters of China

Xiang Weng[1], Jiawei Li[2], Grant L. Forster[1,3], and Peer Nowack[1,4,5]

[1]School of Environmental Sciences, University of East Anglia, Norwich, UK

[2]Key Laboratory of Regional Climate-Environment for Temperate East Asia, Institute of Atmospheric Physics, Chinese Academy of Sciences, Beijing, China

[3]National Centre for Atmospheric Science, University of East Anglia, Norwich, UK

[4]Climatic Research Unit, University of East Anglia, Norwich, UK

[5]Institute of Theoretical Informatics, Karlsruhe Institute of Technology, Karlsruhe, Germany

Contents of this file

Introduction

This supporting information contains details of the model setup and model evaluation, a summary of the projected emission pathways, descriptions of the additional simulations for addressing the effect of aerosols on projected ozone changes, and information regarding how the reaction rate constants for NOx-titration ($NO + O_3 \rightarrow NO_2 + O_2$) and HNO_3 ($OH + NO_2 \rightarrow HNO_3$) formation from the two chemical mechanisms (i.e., MOZART and CBMZ) are calculated and compared.

Text S1. Details of WRF-Chem setup

Simulations using the two chemical mechanisms from WRF-Chem adopt the same setup as described below.

The simulation domain is illustrated in Figure S1. It contains 109 (south–north) × 139 (west–east) horizontal grids at a resolution of 45 km. Vertically, the simulation contains a total of 29 layers from surface level at an average height of about 18 m above ground in eastern China to approximately 50 hPa. The analyses of surface ozone including model evaluation, ozone concentrations in response to 2030 emission changes and perturbations of nitrogen oxides (NO_x), volatile organic compounds (VOCs) emissions are conducted at the lowest model layer.

Simulations for all five emission scenarios (i.e., Base-2017, Limited-controls-2030, Current-goals-2030, Neutral-goals-2030, 1.5℃-goals-2030, see section 2. Materials and methods in the main text and the Text S3 of this document) are conducted for the period from May 29, 2017 to August 31, 2017 with the first three days discarded as model spin-up. Simulations of ozone responses to NO_x and VOCs emission perturbations are conducted for the period from June 28 to July 31, 2017 with the first three days as model spin-up and discarded as well.

Meteorological initial and boundary conditions are provided by National Centers for Environmental Prediction (NCEP) Global Data Assimilation System (GDAS)/final analysis (FNL) (available at https://rda.ucar.edu/datasets/ds083.3/; NCEP, 2015). Global simulation by Community Atmosphere Model with Chemistry (CAM-chem) (available at https://www.acom.ucar.edu/cam-chem/cam-chem.shtml; Lamarque et al., 2012; Emmons et al., 2020) is used for the chemical initial and boundary conditions. Initial and boundary conditions for both meteorology and chemistry reflect the conditions of summer 2017 and remain fixed for all of the emission scenarios. Similar to Silver et al. (2020), nudging of meteorological conditions is only applied above the planetary boundary layer.

The model setup for other modules is mostly based on the settings of Silver et al. (2020) with some further modifications. Specifically, we continue to use the Rapid radiative Transfer Model for GCMs (RRTMG) (Iacono et al., 2008) for both shortwave and longwave radiation simulation, while the Yonsei University (YSU) planetary boundary layer physics scheme (Hong et al., 2006) and thermal diffusion scheme for land-surface physics are adopted. We use Morrison 2-moment (Morrison et al., 2009) for microphysics. Fast-J photolysis scheme is used for efficiently calculating photolysis rates (Wild et al., 2000), and both direct and indirect aerosol-radiation feedback are included.

Text S2. Model evaluation

For evaluating model performance, we use the surface hourly measurement data provided by Ministry of Ecology and Environment (MEE) to compare with simulated O_3, NO_2 and $PM_{2.5}$ from the Base-2017 (using MEIC emission data of 2017 summer) by the two chemical mechanisms. As the main focus of this study is to predict ozone changes given the perturbations of emissions within China, we thus only select stations with reliable ozone observational data following the selection process by Weng et al. (2022) for model evaluation. For pre-processing the observational data, we first spatially average the

measured data from all the available sites within the dimensions of corresponding model grid so that the averaged observational data are spatially matched with the simulated pollutants. Model grids without measurement sites located within are not used for model evaluation. We then calculate the nationwide average model result and observation for each hour during the simulation period (i.e., summer of 2017). The metrics for model evaluation used in this study include normalized mean bias (NMB), mean bias (MB) and Pearson correlation coefficient (r). The calculations of these metrics are documented in Huang et al. (2021), and we summarize them in Table S1. Metrics of NMB, MB and R are estimated based on nationwide averaged hourly model results and observational data.

Results of the model evaluation using these three metrics are summarized in Table S2. In respect of O_3, simulated and observational O_3 are correlated with Pearson correlation coefficients (r) larger than 0.9 for both chemical mechanisms, as illustrated by the linear fittings in Figure S2. Besides, the average diurnal pattern of observational ozone in China can also be captured by both mechanisms (Figure S2c). However, in terms of overall biases in concentration levels, O_3 is overall overestimated by 35.9% (13.0 ppb) in MOZART and a higher overprediction at 39.3% (14.2 ppb) in CBMZ. Using MOZART from WRF-Chem, Silver et al. (2020) reported a roughly 10% underprediction of O_3 on average in China based on the simulation from 2015 to 2017, which is not similar to the overpredictions reported here. The difference of predictive skills between this study and Silver et al. (2020) may be partially due to the difference of simulation period as we conduct model evaluation based on the simulation for summer of 2017 (i.e., Base-2017) while simulation from Silver et al. (2020) covered all seasons from 2015 to 2017. It is also possible that overprediction of ozone may more commonly occur during summer than other seasons (e.g., Tao et al., 2020). Besides, although the emission data we use here is from the same source (i.e., MEIC) as in Silver et al. (2020), we directly adopt MEIC emission data for the year 2017, while Silver et al. (2020) used the emission in 2015 as the base emission and further scaled for 2016 and 2017. This difference can also contribute to the inconsistency of predictive skills since the accuracy of emission data is one of the key factors for model performance (e.g., Huang et al., 2021; Sicard et al., 2021). Apart from hourly ozone, we also assess their predictive skills regarding the maximum daily 8 h average (MDA8) O_3 (also see Table S2). Expectedly, biases in MDA8 O_3 are similar to hourly O_3 but with weaker correlation with observations. Higher Pearson correlation coefficients (R) in hourly O_3 than MDA8 values may be due to the diurnal variation of ozone is included in the hourly data, which is generally easier to be captured by WRF-Chem. Besides, we also provide the comparisons of spatial distributions of observational and modelled MDA8 ozone, as illustrated in Figure S4. The overall spatial distribution of MDA8 O_3 can be reflected by both mechanisms, with less pollution over the southern regions and higher levels in the north. Nevertheless, overprediction of MDA8 ozone is generally found, and such overprediction is more remarkable in CBMZ than MOZART, consistent with the NMB and MB reported in Table S2.

For NO_2, both mechanisms are able to predict the overall concentration level of NO_2 with NMB values of MOZART and CBMZ at 18.8% and -8.92%, respectively. The lower simulated NO_2 in CBMZ than in MOZART may be predominantly due to the stronger HNO_3 formation in CBMZ (see Figure 4 in the main text), i.e., a stronger sink for NO_2. Despite the overall acceptable biases in NO_2 (i.e., NMB within ±20%), we find that there are

overpredictions of NO_2 during nighttime in both mechanisms, which is also reported by Kuik et al. (2016). This overprediction of NO_2 during nighttime may be mainly due to the underestimation of mixing in the boundary layer (Kuik et al., 2016).

As mentioned in the section on Materials and Methods in the main text, Model for Simulating Aerosol Interactions and Chemistry (MOSAIC) coupled with MOZART and CBMZ is used for aerosol simulation. For simplicity, MOZART-MOSAIC and CBMZ-MOSAIC are referred to MOZART and CBMZ herein. With regard to $PM_{2.5}$ simulation, MOZART has a higher overprediction with NMB = 54.6% (MB = 14.8 μg m^{-3}) than CBMZ (NMB = 18.3%, MB = 4.98 μg m^{-3}). Unlike O_3, the overprediction using the MOZART mechanism is also documented by Silver et al. (2020), reporting a similar level of overprediction with NMB = 45%. Interestingly, although the primary emissions of fine particulates are same in both mechanisms, CBMZ shows much lower predicted values than MOZART in this study. One of the main discrepancies regarding aerosol simulation in these two mechanisms is that MOZART includes the simulation of secondary organic aerosol (SOA) formation while CBMZ does not. Based on the simulation of MOZART, we find that the concentrations of SOA in $PM_{2.5}$ fraction can take up about 31% on average over China, and a higher ~40% over eastern China (20–42°N, 110–130°E). Moreover, the SOA fraction can be up to over roughly 60% in regions nearby YRD. This suggests that the high fraction of SOA may be one of the main factors for contributing to the overprediction of $PM_{2.5}$ in MOZART.

In summary, nationwide hourly ozone simulations by either these two mechanisms correlate well with observations. The general diurnal ozone variations can also be captured by these two mechanisms. The overall predictive accuracies (estimated by NMB and MB) for O_3 and $PM_{2.5}$ are reasonable but not ideal, as is typical within CTM simulations of this kind. It should be noted that no observation-based calibration of emission levels is applied to all the emission data used in this study. Therefore, the predictive skills of the simulations here are more prone to emission uncertainties, compared to other studies (e.g., Tan et al., 2015; Zhou et al., 2017; Zheng et al., 2019; An et al., 2021) using more refined emission data for regional/local scale. Besides, in an attempt to improve predictive skill, we conducted various tests including setting different horizontal resolutions of the simulations and adopting different schemes for planetary boundary layer, land-surface physics and radiation. However, no remarkable improvements were found in those tests. Noteworthy, we further conduct simulations using the chemical mechanism of MOZART-GOCART-T1 (also known as MOZCART-T1); significant improvements of both predictive accuracy in O_3 and $PM_{2.5}$ can be found, with NMB for hourly O_3 and $PM_{2.5}$ at 12.9%, -2.4%, respectively. Nationwide hourly simulated ozone by MOZCART-T1 is well correlated with observation (see Figure S3). Spatial distributions and concentration levels of MDA8 ozone by MOZCART-T1 are in good accordance with observations (see Figure S5). Similar to MOZART, ozone increases in urban and industrial regions by 2030 are also predicted by MOZCART-T1 under the scenarios with emission reductions (i.e., Current-goals-2030, Neutral-goals-2030, 1.5℃-goals-2030; see Figure S6). Nevertheless, we decide not to choose this mechanism for our study due to MOZCART-T1's limited considerations in secondary aerosol formation including evolution of nitrate, ammonium. It should be noted that we run MOZCART-T1 using the recommended tropospheric ultraviolet and visible (TUV) photolysis scheme.

Text S3. Summary of the 2030 emission pathways

Emission pathways of "Baseline", "Current-goals", "Ambitious-pollution-Neutral-goals" and "Ambitious-pollution-1.5℃-goals" for the summer of 2030 from Dynamic Projection model for Emissions in China (DPEC) version 1.1 are used in this study. The detailed descriptions of all these pathways are documented by Cheng et al. (2021).

In summary, the pathway of Baseline (denoted as "Limited-controls-2030"in this study to avoid confusion with "Base-2017") represents a scenario that the end-of-pipe emission control measures remain unchanged at the level in 2015, while the Shared Socioeconomic pathway (SSP) is set at SSP4 characterized by highly inequal economic growths and energy demands across regions (Calvin et al., 2017), and the climate-based Representative Concentration Pathways (RCP) is set at 6.0, suggesting relatively unambitious actions in climate policy.

The pathway of Current-goals (termed as Current-goals-2030 herein) assumes China will be able to achieve Nationally Determined Contribution (NDC) pledges by 2030 with the implementations of current released and upcoming end-of-pipe pollution control measures and policies. In this pathway, SSP2 and RCP4.5 are set for socioeconomic drivers and climate constraints, respectively.

Ambitious-pollution-Neutral-goals (i.e., Neutral-goals-2030) represents China's plan for carbon neutrality (i.e., achieving net-zero CO_2 emissions by 2060 as climate constraints) with best available end-of-pipe controls and SSP1 for socioeconomic drivers. The pathway of Ambitious-pollution-1.5℃-goals (i.e., 1.5℃-goals-2030) aims for the pursuit of long-term 1.5℃ temperature limit and air quality improvement by 2060, sharing the same end-of-pipe controls as Neutral-goals-2030, with SSP1 and RCP1.9 as socioeconomic drivers and climate constraints. These two pathways share similar projected emissions of air pollutants given the adoption of identical pollution control technologies (Cheng et al., 2021). However, in terms of CO_2, stronger reduction in 1.5℃-goals-2030 is projected (Cheng et al., 2021) since more ambitious and rapid CO_2 emission reductions may be required for achieving the 1.5℃ goal (Duan et al., 2021).

A comparison of nationwide total emissions of NO_x and non-methane VOC (NMVOC) in boreal summer (June, July, August) for all emission scenarios is illustrated in Figure S7 (the spatial changes of emissions relative to 2017 summer levels are provided in Figure S8). Neutral-goals-2030 and 1.5℃-goals-2030 show equivalent and substantial emission reductions in NO_x and NMVOC compared to Base-2017. Although the NO_x emission reduction in Current-goals-2030 is not as large as Neutral-goals-2030 and 1.5℃-goals-2030, it is still reduced by approximately 41% compared to Base-2017; while the reduction in NMVOC is relatively close to the reduction levels in Neutral-goals-2030 and 1.5℃-goals-2030. On the contrary, Limited-controls-2030 shows emission increases in NO_x and NMVOC relative to 2017 summer levels, and the total increases of NO_x (about 41%) is more pronounced than increases of NMVOC (about 12%).

Text S4. The effects of aerosols on the discrepancies in predicting ozone changes

Cheng et al. (2021) reported substantial changes in $PM_{2.5}$ by 2030 following these emission scenarios. Dramatic increases or decreases in $PM_{2.5}$ concentrations can perturb the radiative balance of the atmosphere or surface (Tian et al., 2019; Zhu et al., 2021) or alter heterogeneous chemistry (Li et al., 2019), thereby affecting ozone concentrations.

However, it is likely that the discrepancies of ozone changes in these two mechanisms are primarily caused by the effects of gas-phase chemistry rather than aerosols. To demonstrate this, we here conduct a set of experiments by running simulations with only considering the gas-phase chemistry. In other words, we completely drop the aerosol schemes from current MOZART and CBMZ simulations. We run the simulations for both Base-2017 and Current-goals-2030 in CBMZ and MOZART during July as this is the typical month for the boreal summer. If aerosols were the dominant cause for the discrepancies in ozone changes, we may see substantial differences in these simulations compared to previous default runs. As shown in Figure S9, although slightly smaller ozone increases are predicted over BTH region by MOZART with only gas-phase chemistry considered, similar ozone discrepancies between these two mechanisms persist, suggesting differences in gas-phase chemistry are the main driver.

Text S5. Reaction rate constants of NO_x-titration and HNO_3 formation

In terms of reaction rate constant for NO_x-titration ($NO + O_3 \rightarrow NO_2 + O_2$), calculations in both mechanisms follow the same Arrhenius expression (e.g., DeMore et al., 1997):

$$k = A \cdot \exp\left(\frac{-E}{RT}\right)$$

Where k is the rate constant; A denotes the frequency factor; E represents the activation energy; R is the ideal gas law constant and T is the absolute temperature (Brauner & Shacham, 1997). Based on the expression, the rate constant of NO_x-titration is temperature dependent. In MOZART, A is set at 3×10^{-12}, and $\frac{E}{R}$ is 1500 (Emmons et al., 2010), whereas A is 2×10^{-12} and $\frac{E}{R}$ is 1400 in CBMZ (Zaveri & Peters, 1999). This gives MOZART a higher reaction rate constant than CBMZ from temperature above 246.63 K. For example, given temperature at 298 K, the rate constant for MOZART is 1.95×10^{-14} cm^3 $molecules^{-1}$ s^{-1} which is higher than 1.82×10^{-14} cm^3 $molecules^{-1}$ s^{-1} for CBMZ. Figure S10 illustrates the two mechanisms' reaction rate constants of NO_x-titration in response to the changes of temperature from 273 to 313 K, further highlighting a higher rate constant in MOZART within a wide range of temperature.

For rate constant of HNO_3 formation (i.e., $OH + NO_2 \rightarrow HNO_3$), the calculations for both mechanisms are illustrated as below in the form of Troe expression, which can also be referred to DeMore et al. (1997) and Sun et al. (2022):

$$k = \left(\frac{k_0(T)[M]}{1 + \left(k_0(T)[M]/k_\infty(T)\right)}\right)0.6^{\left\{1+\left[\log_{10}\left(\frac{k_0(T)[M]}{k_\infty(T)}\right)\right]^2\right\}^{-1}}$$

Where $[M]$ is the air concentration in unit of molecule cm^{-3}. The value of [M] can be approximately derived from the ideal gas law. For example, under 1 atm and 298 K conditions, the concentration of air molecules is 2.46×10^{19} molecules cm^{-3}. From the equation above, $k_0(T)$ is the low-pressure limiting rate constant, whereas $k_\infty(T)$ is the high-pressure limiting rate constant. Both $k_0(T)$ and $k_\infty(T)$ are temperature-dependent, and their functions of temperature can be expanded as below:

$$k_0(T) = k_0^{300}(T/300)^{-n}$$

$$k_\infty(T) = k_\infty^{300}(T/300)^{-m}$$

In MOZART, k_0^{300} = 2.0×10^{-30}, n = 3, k_∞^{300} = 2.5×10^{-11}, m=0 (Emmons et al., 2010; Sander et al., 2003), whereas k_0^{300}= 2.5×10^{-30}, n = 4.4, k_∞^{300}= 1.6×10^{-11}, m=1.7 in CBMZ (Zaveri & Peters, 1999). Therefore, with $[M]$ = 2.46×10^{19} molecules cm^{-3} s^{-1} at 298 K and 1 atm, the reaction rate constant of HNO_3 formation for MOZART is 1.05×10^{-11} cm^3 $molecules^{-1}$ s^{-1}, which is higher than 8.83×10^{-12} cm^3 $molecules^{-1}$ s^{-1} in CBMZ. The higher reaction rate constant in MOZART than CBMZ is also reported by Visser et al. (2019).

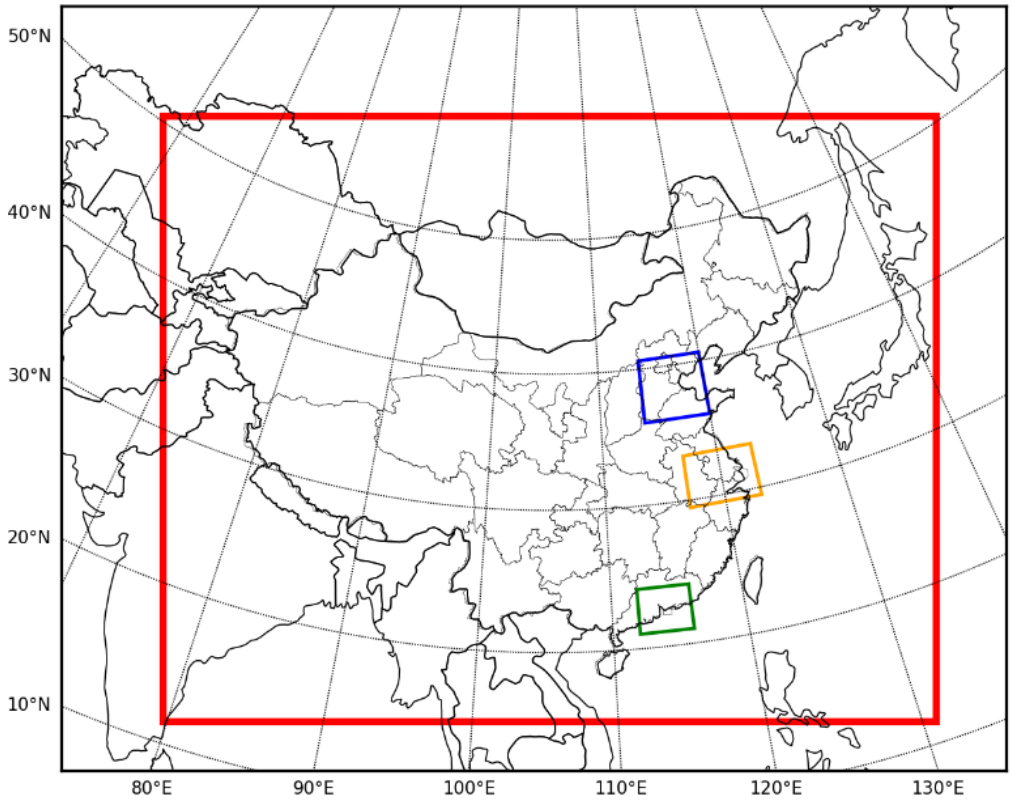

Figure S1. The domain of WRF-Chem simulation (red) and the regions of three key megacity cluster regions with high population density, Beijing–Tianjin–Hebei (BTH, blue box; 114–120°E, 36–40.62°N), Yangtze River Delta (YRD, orange box; 117–123°E, 29.458–33.238°N), Pearl River Delta (PRD, green box; 112–116°E, 21–24.111°N). The boundaries of the city cluster regions are the same as in Weng et al. (2022).

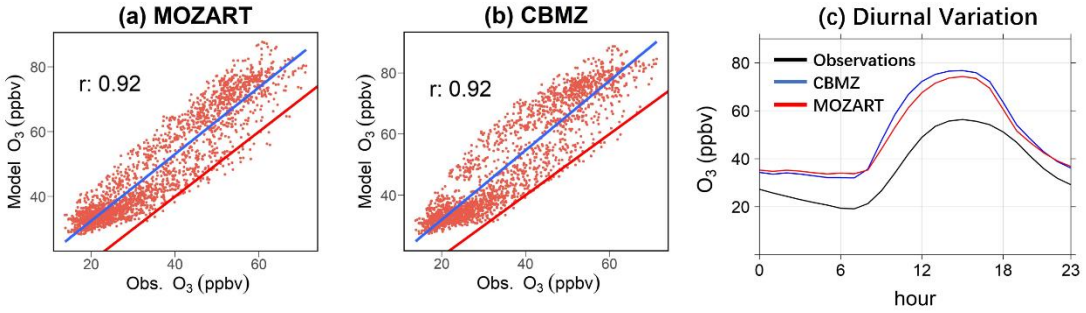

Figure S2. Comparison of nationwide hourly ozone between model predictions and observations for MOZART (a) and CBMZ (b) during summer of 2017 (Base-2017). Blue lines represent the linear fits; red lines are the 1:1 lines. Insert values are Pearson correlation coefficients (r). The nationwide average diurnal variation of ozone for both mechanisms and observations is shown in (c).

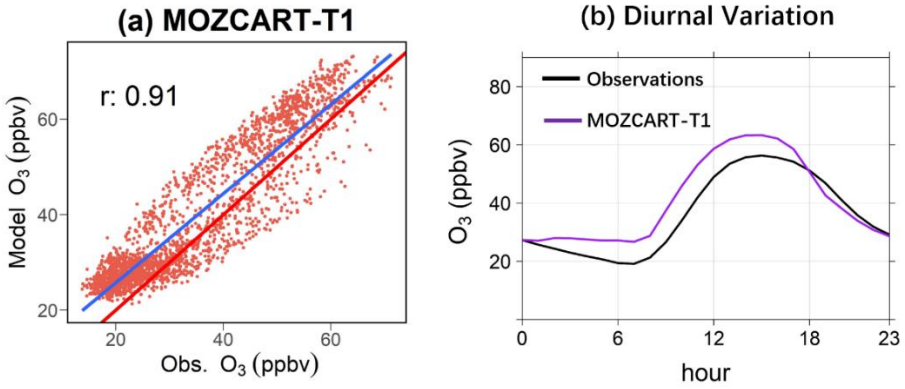

Figure S3. Same as Figure S2, but for MOZCART-T1 mechanism.

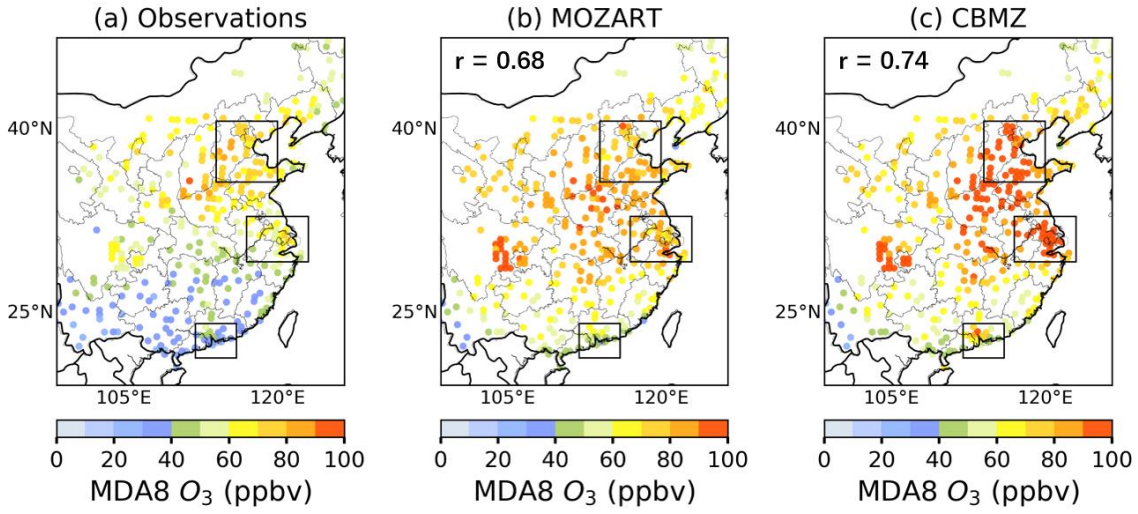

Figure S4. Spatial distributions of summertime average MDA8 ozone in 2017. Panel (a) shows observational values. Panel (b) and (c) show simulated values by MOZART and CBMZ, respectively. Spatial correlation coefficients (r) are inserted at the top left corner of panel (b) and (c). Each point represents the center of a model grid location. Observational MDA8 ozone are spatially averaged over each corresponding model grid location.

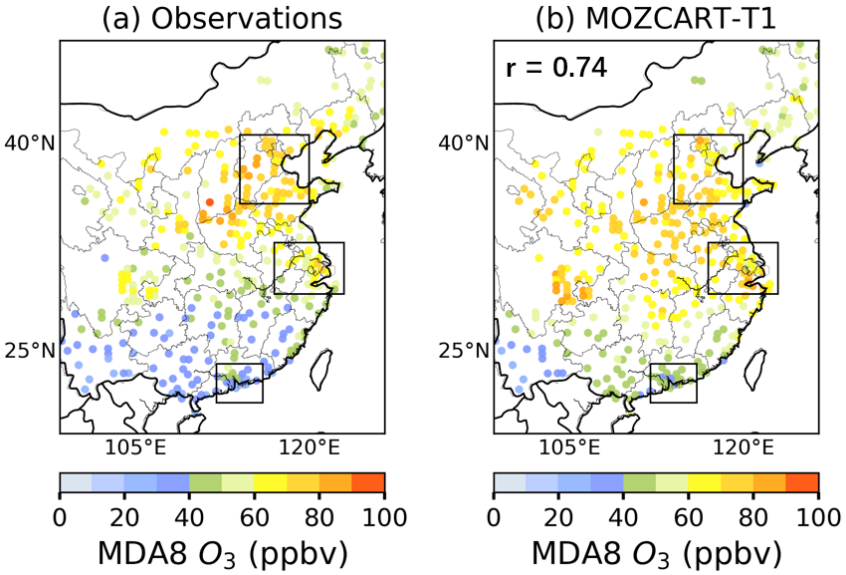

Figure S5. Same as Figure S4, but for MOZCART-T1 mechanism.

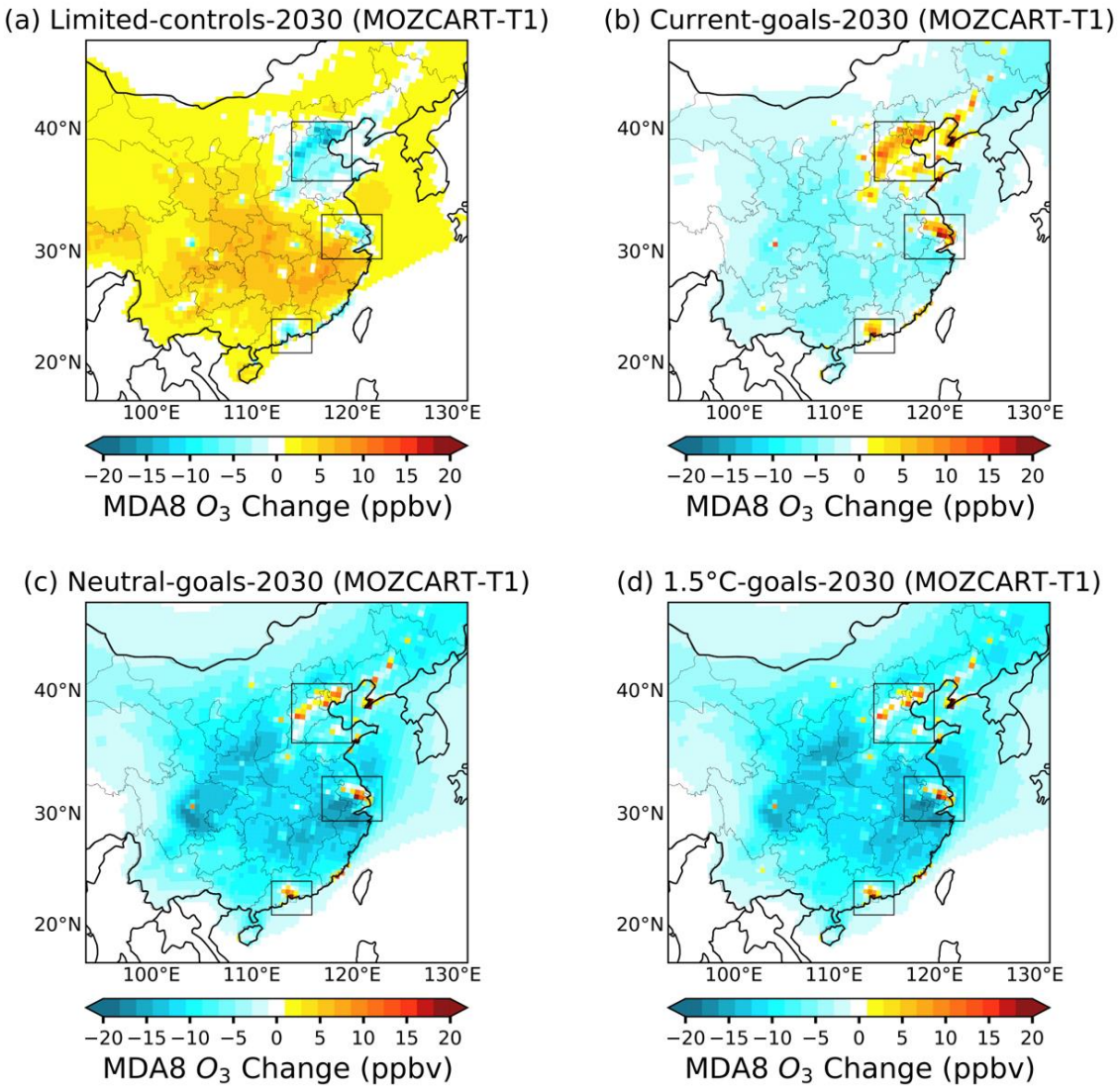

Figure S6. Simulated summertime average MDA8 ozone changes by MOZCART-T1 for each emission scenario for the year 2030, relative to Base-2017 levels.

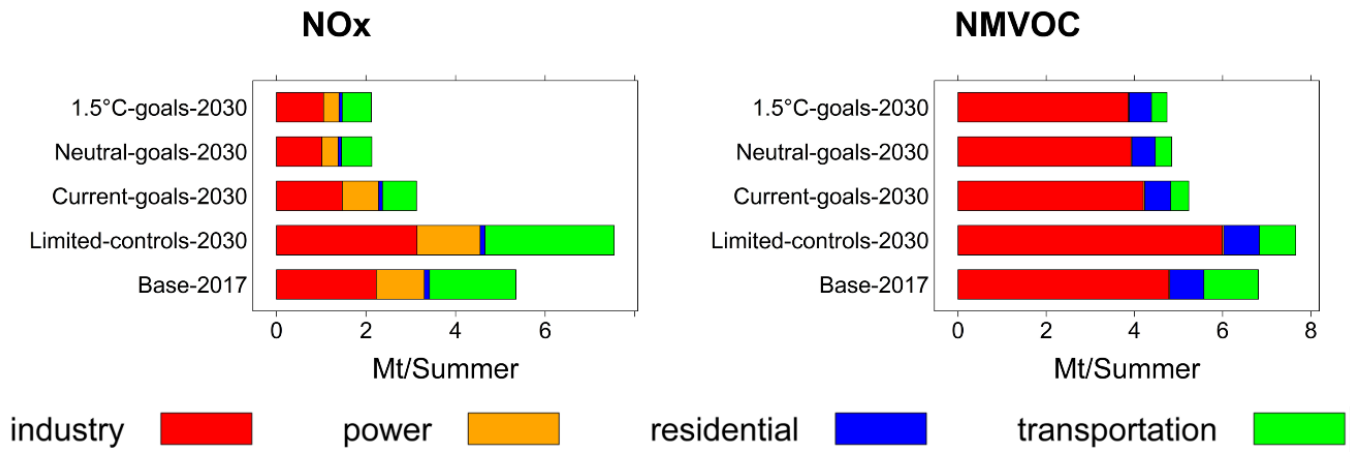

Figure S7. Nationwide total emissions of anthropogenic NOx, NMVOC by sectors during summer for all emission scenarios in this study.

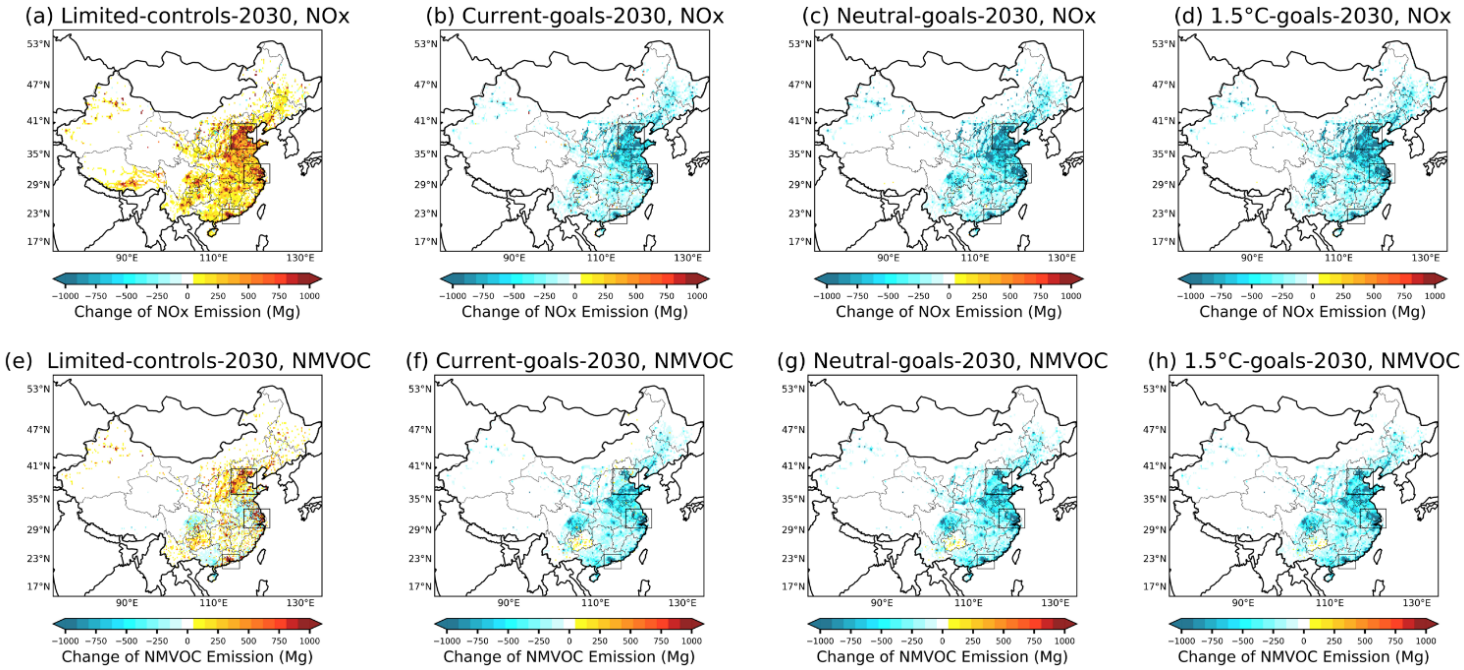

Figure S8. Changes of summertime NOx (a–d), NMVOC (e–h) emissions in 2030 emission scenarios relative to 2017 summer levels (Base-2017). The grid boxes in each subplot represent the three key megacity clusters of China.

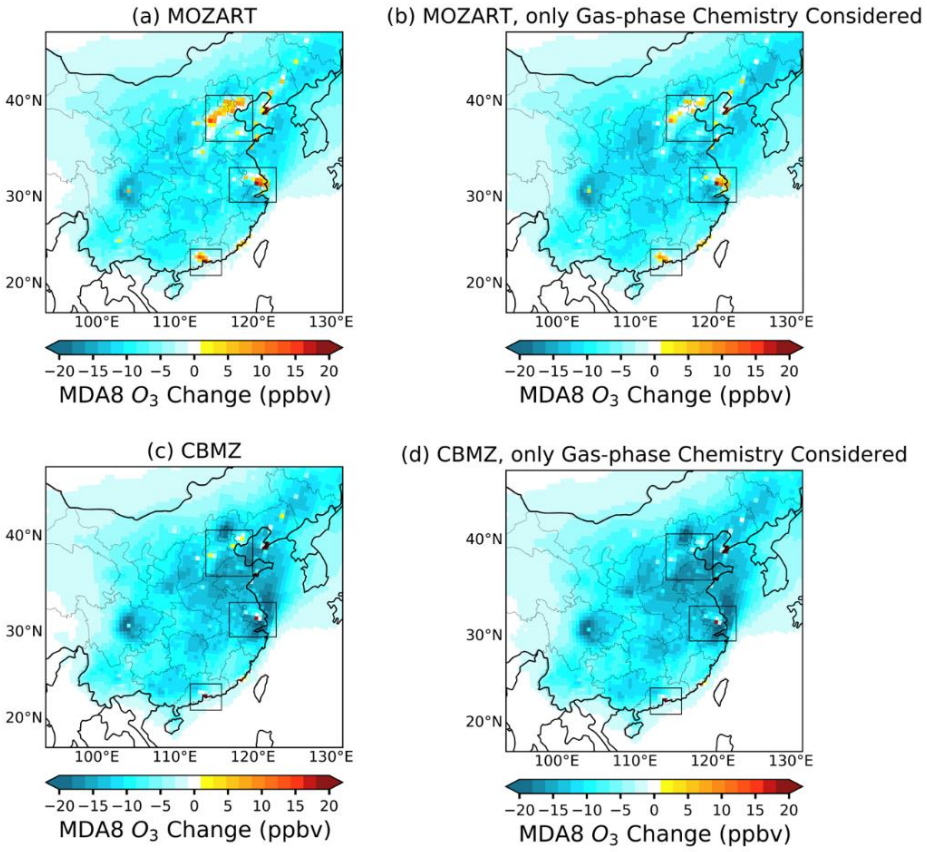

Figure S9. Simulated average MDA8 ozone changes in July for Current-goals-2030, relative to Base-2017 levels. The default simulations with MOZART(a). The same as (a) but with only gas-phase chemistry being considered (b). The default simulations with CBMZ(c). The same as (c) but with but with only gas-phase chemistry being considered (d).

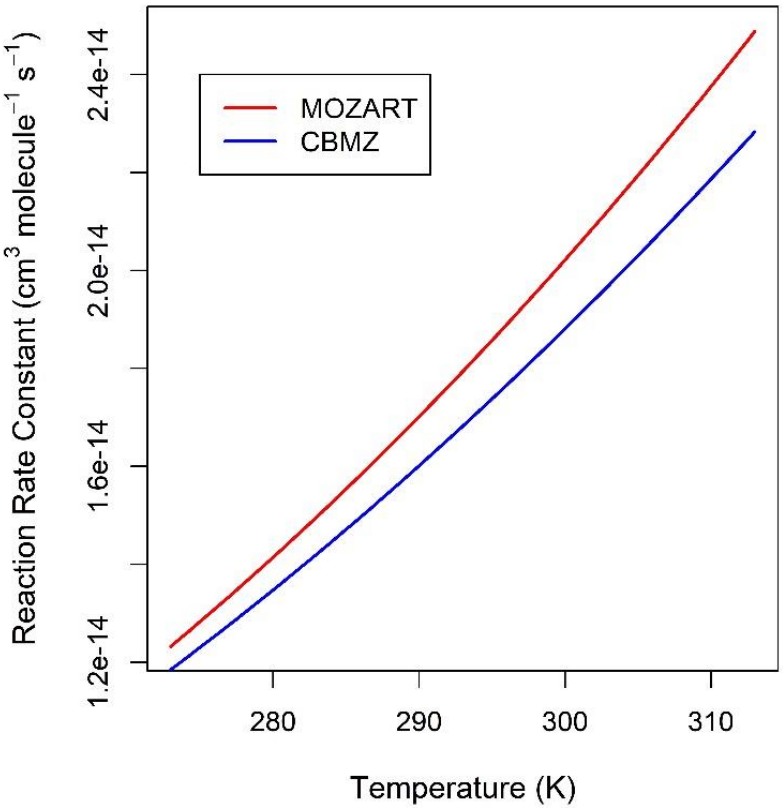

Figure S10. The reaction rate constant of NO + O_3 → NO_2 + O_2 as a function of temperature in MOZART (red) and CBMZ (blue).

Table S1. Statistical metrics for NMB, MB and r. $\boldsymbol{P_j}$ and$\boldsymbol{O_j}$ are nationwide averaged hourly model and observational values, respectively.

Statistics (abbreviation)	Algorithm
Normalized mean bias (NMB)	$\frac{\sum(P_j - O_j)}{\sum O_j} \times 100\%$
Mean bias (MB)	$\frac{\sum(P_j - O_j)}{N}$
Pearson correlation coefficient (r)	$\frac{\sum[(P_j - \overline{P}) \times (O_j - \overline{O})]}{\sqrt{\sum(P_j - \overline{P})^2 \times \sum(O_j - \overline{O})^2}}$

Table S2. Performance statistics for O_3, MDA8 O_3, NO_2 and $PM_{2.5}$ simulations by the two chemical mechanisms against observations. NMB and r are unitless, while unit of MB is ppbv for O_3, NO_2, and μg m^{-3} for $PM_{2.5}$.

Metrics	Mechanisms	O_3	MDA8 O_3	NO_2	$PM_{2.5}$
NMB	MOZART	35.9%	29.7%	18.8%	54.6%
	CBMZ	39.3%	35.8%	-8.92%	18.3%
MB	MOZART	13.0	16.1	2.10	14.8
	CBMZ	14.2	19.4	-1.00	4.98
r	MOZART	0.92	0.71	0.75	0.37
	CBMZ	0.92	0.71	0.65	0.41

References:

An, J., Huang, Y., Huang, C., Wang, X., Yan, R., Wang, Q., Wang, H., Jing, S. ao, Zhang, Y., Liu, Y., Chen, Y., Xu, C., Qiao, L., Zhou, M., Zhu, S., Hu, Q., Lu, J., & Chen, C. (2021). Emission inventory of air pollutants and chemical speciation for specific anthropogenic sources based on local measurements in the Yangtze River Delta region, China. *Atmospheric Chemistry and Physics*, *21*(3), 2003–2025. https://doi.org/10.5194/acp-21-2003-2021

Brauner, N., & Shacham, M. (1997). Statistical analysis of linear and nonlinear correlation of the Arrhenius equation constants. *Chemical Engineering and Processing: Process Intensification*, *36*(3), 243–249. https://doi.org/10.1016/S0255-2701(96)04186-4

Calvin, K., Bond-Lamberty, B., Clarke, L., Edmonds, J., Eom, J., Hartin, C., Kim, S., Kyle, P., Link, R., Moss, R., McJeon, H., Patel, P., Smith, S., Waldhoff, S., & Wise, M. (2017). The SSP4: A world of deepening inequality. *Global Environmental Change*, *42*, 284–296. https://doi.org/10.1016/j.gloenvcha.2016.06.010

Cheng, J., Tong, D., Zhang, Q., Liu, Y., Lei, Y., Yan, G., Yan, L., Yu, S., Cui, R. Y., Clarke, L., Geng, G., Zheng, B., Zhang, X., Davis, S. J., & He, K. (2021). Pathways of China's PM2.5 air quality 2015–2060 in the context of carbon neutrality. *National Science Review*, *8*(nwab078). https://doi.org/https://doi.org/10.1093/nsr/nwab078

DeMore, W. B., Sander, S. P., Golden, D. M., Hampson, R. F., Kurylo, M. J., Howard, C. J., Ravishankara, A. R., Kolb, C. E., & Molina, M. J. (1997). Chemical kinetics and photochemical data for use in stratospheric modeling Evaluation Number 12. In *JPL publication 97-4*.

Duan, H., Zhou, S., Jiang, K., Bertram, C., Harmsen, M., Kriegler, E., van Vuuren, D. P., Wang, S., Fujimori, S., Tavoni, M., Ming, X., Keramidas, K., Iyer, G., & Edmonds, J. (2021). Assessing China's efforts to pursue the 1.5°C warming limit. *Science*, *372*(6540), 378–385. https://doi.org/10.1126/science.aba8767

Emmons, L. K., Schwantes, R. H., Orlando, J. J., Tyndall, G., Kinnison, D., Lamarque, J. F., Marsh, D., Mills, M. J., Tilmes, S., Bardeen, C., Buchholz, R. R., Conley, A., Gettelman, A., Garcia, R., Simpson, I., Blake, D. R., Meinardi, S., & Pétron, G. (2020). The Chemistry Mechanism in the Community Earth System Model Version 2 (CESM2). *Journal of Advances in Modeling Earth Systems*, *12*(4), 1–21. https://doi.org/10.1029/2019MS001882

Emmons, L. K., Walters, S., Hess, P. G., Lamarque, J. F., Pfister, G. G., Fillmore, D., Granier, C., Guenther, A., Kinnison, D., Laepple, T., Orlando, J., Tie, X., Tyndall, G., Wiedinmyer, C., Baughcum, S. L., & Kloster, S. (2010). Description and evaluation of the Model for Ozone and Related chemical Tracers, version 4 (MOZART-4). *Geoscientific Model Development*, *3*(1), 43–67. https://doi.org/10.5194/gmd-3-43-2010

Hong, S. Y., Noh, Y., & Dudhia, J. (2006). A new vertical diffusion package with an explicit treatment of entrainment processes. *Monthly Weather Review*, *134*(9), 2318–2341. https://doi.org/10.1175/MWR3199.1

Huang, L., Zhu, Y., Zhai, H., Xue, S., Zhu, T., Shao, Y., Liu, Z., Emery, C., Yarwood, G., Wang, Y., Fu, J., Zhang, K., & Li, L. (2021). Recommendations on benchmarks for numerical

air quality model applications in China - Part 1: PM2.5 and chemical species. *Atmospheric Chemistry and Physics*, *21*(4), 2725–2743. https://doi.org/10.5194/acp-21-2725-2021

Iacono, M. J., Delamere, J. S., Mlawer, E. J., Shephard, M. W., Clough, S. A., & Collins, W. D. (2008). Radiative forcing by long-lived greenhouse gases: Calculations with the AER radiative transfer models. *Journal of Geophysical Research Atmospheres*, *113*(13), 2–9. https://doi.org/10.1029/2008JD009944

Kuik, F., Lauer, A., Churkina, G., Denier Van Der Gon, H. A. C., Fenner, D., Mar, K. A., & Butler, T. M. (2016). Air quality modelling in the Berlin-Brandenburg region using WRF-Chem v3.7.1: Sensitivity to resolution of model grid and input data. *Geoscientific Model Development*, *9*(12), 4339–4363. https://doi.org/10.5194/gmd-9-4339-2016

Lamarque, J. F., Emmons, L. K., Hess, P. G., Kinnison, D. E., Tilmes, S., Vitt, F., Heald, C. L., Holland, E. A., Lauritzen, P. H., Neu, J., Orlando, J. J., Rasch, P. J., & Tyndall, G. K. (2012). CAM-chem: Description and evaluation of interactive atmospheric chemistry in the Community Earth System Model. *Geoscientific Model Development*, *5*(2), 369–411. https://doi.org/10.5194/gmd-5-369-2012

Li, K., Jacob, D. J., Liao, H., Shen, L., Zhang, Q., & Bates, K. H. (2019). Anthropogenic drivers of 2013–2017 trends in summer surface ozone in China. *Proceedings of the National Academy of Sciences of the United States of America*, *116*(2), 422–427. https://doi.org/10.1073/pnas.1812168116

Morrison, H., Thompson, G., & Tatarskii, V. (2009). Impact of cloud microphysics on the development of trailing stratiform precipitation in a simulated squall line: Comparison of one- and two-moment schemes. *Monthly Weather Review*, *137*(3), 991–1007. https://doi.org/10.1175/2008MWR2556.1

NCEP. (2015). *NCEP GDAS/FNL 0.25 Degree Global Tropospheric Analyses and Forecast Grids, Research Data Archive at the National Center for Atmospheric Research, Computational and Information Systems Laboratory*. https://doi.org//10.5065/D65Q4T4Z

Sander, S. P., Friedl, R. R., Ravishankara, A. R., Golden, D. M., Kolb, C. E., Kurylo, M. J., Huie, R. E., Orkin, V. L., Molina, M. J., Moortgat, G. K., & Finlayson-Pitts, B. J. (2003). *Chemical Kinetics and Photochemical Data for Use in Atmospheric Studies, evaluation number 14*. JPL publication 02-25.

Sicard, P., Crippa, P., De Marco, A., Castruccio, S., Giani, P., Cuesta, J., Paoletti, E., Feng, Z., & Anav, A. (2021). High spatial resolution WRF-Chem model over Asia: Physics and chemistry evaluation. *Atmospheric Environment*, *244*(October 2020), 118004. https://doi.org/10.1016/j.atmosenv.2020.118004

Silver, B., Conibear, L., Reddington, C. L., Knote, C., Arnold, S. R., & Spracklen, D. V. (2020). Pollutant emission reductions deliver decreased PM2.5-caused mortality across China during 2015-2017. *Atmospheric Chemistry and Physics*, *20*(20), 11683–11695. https://doi.org/10.5194/acp-20-11683-2020

Sun, L., Cao, L., Ding, H., Gao, M., Li, S., & Chen, G. (2022). Influence of using different chemical mechanisms on simulations of ozone and its precursors in the troposphere

of Shanghai , China. *Atmospheric Environment*, *289*(August), 119299. https://doi.org/10.1016/j.atmosenv.2022.119299

Tan, J., Zhang, Y., Ma, W., Yu, Q., Wang, J., & Chen, L. (2015). Impact of spatial resolution on air quality simulation: A case study in a highly industrialized area in Shanghai, China. *Atmospheric Pollution Research*, *6*(2), 322–333. https://doi.org/10.5094/APR.2015.036

Tao, Z., Chin, M., Gao, M., Kucsera, T., Kim, D., Bian, H., Kurokawa, J. I., Wang, Y., Liu, Z., Carmichael, G. R., Wang, Z., & Akimoto, H. (2020). Evaluation of NU-WRF model performance on air quality simulation under various model resolutions - An investigation within the framework of MICS-Asia Phase III. *Atmospheric Chemistry and Physics*, *20*(4), 2319–2339. https://doi.org/10.5194/acp-20-2319-2020

Tian, R., Ma, X., Jia, H., Yu, F., Sha, T., & Zan, Y. (2019). Aerosol radiative effects on tropospheric photochemistry with GEOS-Chem simulations. *Atmospheric Environment*, *208*(March), 82–94. https://doi.org/10.1016/j.atmosenv.2019.03.032

Visser, A. J., Folkert Boersma, K., Ganzeveld, L. N., & Krol, M. C. (2019). European NOx emissions in WRF-Chem derived from OMI: Impacts on summertime surface ozone. *Atmospheric Chemistry and Physics*, *19*(18), 11821–11841. https://doi.org/10.5194/acp-19-11821-2019

Weng, X., Forster, G. L., & Nowack, P. (2022). A machine learning approach to quantify meteorological drivers of ozone pollution in China from 2015 to 2019. *Atmospheric Chemistry and Physics*, *22*(12), 8385–8402. https://doi.org/10.5194/acp-22-8385-2022

Wild, O., Zhu, X., & Prather, M. J. (2000). Fast-J: Accurate simulation of in- and below-cloud photolysis in tropospheric chemical models. *Journal of Atmospheric Chemistry*, *37*(3), 245–282. https://doi.org/10.1023/A:1006415919030

Zaveri, R. A., & Peters, L. K. (1999). A new lumped structure photochemical mechanism for large-scale applications. *Journal of Geophysical Research: Atmospheres*, *104*(D23), 30387–30415. https://doi.org/https://doi.org/10.1029/1999JD900876

Zheng, H., Cai, S., Wang, S., Zhao, B., Chang, X., & Hao, J. (2019). Development of a unit-based industrial emission inventory in the Beijing-Tianjin-Hebei region and resulting improvement in air quality modeling. *Atmospheric Chemistry and Physics*, *19*(6), 3447–3462. https://doi.org/10.5194/acp-19-3447-2019

Zhou, Y., Zhao, Y., Mao, P., Zhang, Q., Zhang, J., Qiu, L., & Yang, Y. (2017). Development of a high-resolution emission inventory and its evaluation and application through air quality modeling for Jiangsu Province, China. *Atmospheric Chemistry and Physics*, *17*(1), 211–233. https://doi.org/10.5194/acp-17-211-2017

Zhu, J., Chen, L., Liao, H., Yang, H., Yang, Y., & Yue, X. (2021). Enhanced PM2.5 Decreases and O3 Increases in China During COVID-19 Lockdown by Aerosol-Radiation Feedback. *Geophysical Research Letters*, *48*(2). https://doi.org/10.1029/2020GL090260